

Diffusive transport in the lowest Landau level of disordered 2d semimetals: the mean-square-displacement approach

Andreas Sinner, Gregor Tkachov

Angaben zur Veröffentlichung / Publication details:

Sinner, Andreas, and Gregor Tkachov. 2022. "Diffusive transport in the lowest Landau level of disordered 2d semimetals: the mean-square-displacement approach." *The European Physical Journal B* 95 (6): 95. <https://doi.org/10.1140/epjb/s10051-022-00358-1>.



Diffusive transport in the lowest Landau level of disordered 2d semimetals: the mean-square-displacement approach

Andreas Sinner^{1,2,a}  and Gregor Tkachov¹ 

¹ Institut für Physik, Universität Augsburg, 86135 Augsburg, Germany

² Instytut Fizyki, Uniwersytet Opolski, 45-052 Opole, Poland

Received 24 February 2022 / Accepted 23 May 2022
© The Author(s) 2022

Abstract. We study the electronic transport in the lowest Landau level of disordered two-dimensional semimetals placed in a homogeneous perpendicular magnetic field. The material system is modeled by the Bernevig–Hughes–Zhang Hamiltonian, which has zero energy Landau modes due to the material's intrinsic Berry curvature. These turn out to be crucially important for the density of states and the static conductivity of the disordered system. We develop an analytical approach to the diffusion and conductivity based on a self-consistent equation of motion for the mean-squared displacement. The obtained value of the zero mode conductivity is close to the conductivity of disordered Dirac electrons without magnetic fields, which have zero energy points in the spectrum as well. Our analysis is applicable in a broader context of disordered two-dimensional electron gases in strong magnetic fields.

1 Introduction

The subjects of low-dimensional semimetals and related topics of topological states of matter and spintronics have witnessed an enormous boom during the last decades [1–7]. In magnetic fields, the quantum mechanics of charge carriers in these materials is governed by a spectacular interplay of the intrinsic and magnetic field-induced Berry curvatures. Several aspects of this fascinating physics remain widely untouched, though. For instance, relatively little is known about the role of disorder and its interplay with the magnetic field. The overall progress in this area has been slow, not least because of the technical challenges, considerable even by the standards of the community [8–12]. There are a number of issues which make the disordered electrons in the homogeneous perpendicular magnetic field look differently as compared to the situation without a magnetic field. Due to the freedom of the gauge choice, the problem can be approached in a number of ways, which differ very much in detail. For instance, the choice of the central gauge has the advantage that the solutions of the Schrödinger equation are states localized in the space. Therefore, one can do computations in the position space in an exact manner. The envisaged problem is notoriously difficult because the model lacks a small expansion parameter [13]. This inevitably leads to divergent expansion series. A powerful method to keep such divergences under control is the

renormalization group. In the past, our understanding of the physics of disordered metals and semiconductors profited vastly from the various combinations of variational and perturbative techniques with the renormalization group, c.f. Refs. [14–19] and Refs. [20–22].

However, in the central gauge picture, there is literally no continuous variable to be sliced off by iterations to obtain the renormalization group equations. Of course, one can use a different gauge, which allows for description in terms of states localized in one direction and propagating in the other. The price to pay is the loss of exactness, which is too costly to give up. In this paper, we develop a diagrammatic approach to the conductivity of the two-dimensional disordered electron gas in a strong magnetic field in the central gauge picture. While these series can still be wrapped up exactly for the single-particle propagators, as it was impressively demonstrated by Wegner in Ref. [9], additional technical issues make every attempt of applying these techniques to the two-particle propagators elusive. The available divergent series cannot be directly plugged into the Kubo formula without some not a priori obvious sort of regularization or resummation. Hence, the usual way to approach the conductivity is via the Einstein relation and correspondingly via the notion of diffusion [23–25]. Because the corresponding statistical averages require normalization with respect to the vacuum fluctuations [26], this provides a tool for estimating the measurable quantities by means of some kind of analytical continuation [11, 12, 27, 28].

Our approach may not differ much from the others in relying on perturbative expansions for the

^a e-mail: andreas.sinner@physik.uni-augsburg.de (corresponding author)

two-particle propagator. It too requires as much information from the perturbative expansion as possible and so we perform the exact computations of perturbative series to the practical limits of doable. Moreover, we even go beyond that. We classify diagrammatic channels according to their behavior on large scales in the position space and identify the dominant ones. In principle, this gives a hint toward the exact asymptotics of the correlation functions. What is different in our work is the way we approach the mean-squared displacement and from this the diffusion coefficient. Instead of resumming the perturbative series, our departing point is the individual behavior in time of each element of the perturbative series. It turns out that the behavior at larger time is dominated by the higher-order elements and tends toward a stationary state. On the sublaying time scales though, there is a large region with linear time dependence, characteristic of the diffusion. To approach this regime, we propose a self-consistent equation of motion for the mean-squared displacement and extract the diffusion coefficient from there. With the obtained diffusion coefficient and density of states, we find via the Einstein relation a universal expression for the static conductivity in the lowest Landau level.

For concreteness we chose the Hamiltonian proposed by Bernevig, Hughes and Zhang in the context of the quantum spin Hall effect [7, 29]. Its spectral properties are well known and thoroughly studied in the cited literature. The distinctive feature of the BHZ-Hamiltonian in the lowest Landau level is the appearance of states with zero energy at a certain strength of the magnetic field. These Landau zero modes prove crucial to the transport in the presence of disorder. Both the density of states and the conductivity obtained from the Einstein relation are peaked around these modes. In all, the system becomes metallic within a parameter window around them, which becomes broader but also less expressed with increasing disorder. The numerical value exactly at a zero point is close to that of Dirac electrons in random potentials.

The paper is organized as follows. In Sect. 2 we specify the microscopic BZH-Hamiltonian which we use for concrete discussions. We discuss the specifics of its spectrum and eigenstates, and introduce the corresponding Green's function in Sect. 3. In Sect. 4, we discuss the effect of the different types of disorder and the density of states. In Sect. 5, we discuss the mean-squared displacement and its relation to the diffusion. We present an explicit evaluation of the mean-squared displacement to any finite order in perturbative expansion. For this, we determine an exact asymptotic expression for the two-particle propagators. In Sect. 6, we propose a self-consistent equation of motion for the mean-squared displacement and extract the diffusion coefficient from that. This gives us an access to the static conductivity. Lengthy auxiliary calculation pieces are moved into the Appendix.

2 The model Hamiltonian

In the absence of magnetic field, the BHZ-Hamiltonian reads

$$H = \Delta_0 \Sigma_{03} - \epsilon_0 \Sigma_{00} - (\mathcal{C}_+ T_- + \mathcal{C}_- T_+) \nabla_+ \nabla_- - iv (\mathcal{D}_+ \nabla_- + \mathcal{D}_- \nabla_+). \quad (1)$$

the Hamiltonian is shown in its explicit form in Appendix 1. The shorthands used here are $\nabla_{\pm} = \partial_x \pm i\partial_y$, $\nabla_+ \nabla_- = \partial_x^2 + \partial_y^2$, $T_{\pm} = \frac{1}{2m} \pm B_0$. The 4×4 matrix body of the Hamiltonian is spanned by some of the 16 Dirac matrices $\Sigma_{ab} = \sigma_a \otimes \sigma_b$, the first index referring to the spin space, $a, b = 0, 1, 2, 3$, with $\sigma_{a=1,2,3}$ denoting the Pauli matrices in their usual representation and $\sigma_{a=0}$ being the two-dimensional unity matrix. With this, the matrices \mathcal{C}_{\pm} and \mathcal{D}_{\pm} read

$$\mathcal{C}_{\pm} = \frac{1}{2} [\Sigma_{00} \pm \Sigma_{03}], \quad \text{and} \quad \mathcal{D}_{\pm} = \frac{1}{2} [\Sigma_{01} \pm i\Sigma_{02}]. \quad (2)$$

The band gap Δ_0 is supposed to be much smaller than the typical gap in 2d semiconductors. For instance, for the BHZ-Hamiltonian adopted to HgTe quantum wells $\Delta_0 \sim 10$ meV [7].

We emphasize that even though we frequently use expressions like 'spin and its projections', we do not always mean the physical spin of the electron. For graphene or other systems which host Weyl or Dirac fermions, it is better to think of the valley or sublattice degrees of freedom, rather than the electron spin. It is mainly due to the established tradition that we use this vocabulary.

In strong magnetic field we replace the usual derivatives by the covariant ones $\partial_{\mu} \rightarrow \partial_{\mu} + iA_{\mu}$, with the vector potential A related to the magnetic field via $\nabla \times A = B$. This condition can be realized by a number of gauges. We will use the central gauge

$$A = \frac{B}{2} \begin{pmatrix} -y \\ x \\ 0 \end{pmatrix}, \quad (3)$$

the choice which makes analytical calculations particularly convenient. Introducing complex coordinates $z = x + iy$, $\bar{z} = x - iy$, and corresponding derivatives $\partial_z = (\partial_x - i\partial_y)/2$, $\partial_{\bar{z}} = (\partial_x + i\partial_y)/2$, with the properties $\partial_z z = \partial_{\bar{z}} \bar{z} = 1$, $\partial_z \bar{z} = \partial_{\bar{z}} z = 0$, we get $\nabla_- \rightarrow 2\partial_z + k^2 \bar{z} = A$, $\nabla_+ \rightarrow 2\partial_{\bar{z}} - k^2 z = A^{\dagger}$, and $\nabla_+ \nabla_- \rightarrow (2\partial_{\bar{z}} - k^2 z)(2\partial_z + k^2 \bar{z}) - 2k = A^{\dagger} A - 2k$, where

$$k^2 = \frac{eB}{2\hbar} = \frac{1}{\ell^2}. \tag{4}$$

$\ell = 1/k$ is referred to as the magnetic length. The operator A annihilates the functions

$$\varphi_n(r) = \frac{k}{\sqrt{\pi}} \frac{(k\bar{z})^n}{\sqrt{n!}} e^{-\frac{k^2}{2}z\bar{z}}, \tag{5}$$

i.e., $A\varphi_n(r) = 0$, for every positive integer n . Hence, $\varphi_n(r)$ is the lowest Landau level eigenfunction of the conventional operator of kinetic energy $\propto A^\dagger A$. The Hilbert space of the lowest Landau level is infinitely degenerate, i.e., n can assume every positive integer value between zero and infinity.

In this notation, the Hamiltonian becomes

$$H = \Delta\Sigma_{03} - \epsilon_0\Sigma_{00} + 2k(C_+T_- + C_-T_+) - (C_+T_- + C_-T_+)A^\dagger A - iv(D_+A + D_-A^\dagger). \tag{6}$$

The ground state (i.e., the eigenstate in the lowest Landau level) suffices the condition

$$[(C_+T_- + C_-T_+)A^\dagger A + iv(D_+A + D_-A^\dagger)]\psi = 0, \tag{7}$$

which suggests two solutions:

$$\psi_{+,n}(r) = \varphi_n(r) \begin{pmatrix} 0 \\ 1 \\ 0 \\ 0 \end{pmatrix}, \quad \psi_{-,n}(r) = \varphi_n(r) \begin{pmatrix} 0 \\ 0 \\ 1 \\ 0 \end{pmatrix}, \tag{8}$$

which are unique up to a global phase and correspond to the two spin polarizations. The respective eigenvalues of the Hamiltonian for each spin projection in the lowest Landau level are found from the stationary Schrödinger equation

$$H\psi = E\psi, \tag{9}$$

which yields for both spectral branches [7]

$$E_+ = 2T_+k - \epsilon_0 - \Delta_0, \quad E_- = 2T_-k - \epsilon_0 + \Delta_0. \tag{10}$$

The existence of zero energy points is due to model's intrinsic Berry curvature [29]. In general, both eigenvalues may become zero at different magnetic fields:

$$E_\pm = 0 \text{ for } k_\pm = \frac{\epsilon_0 \pm \Delta_0}{2T_\pm}. \tag{11}$$

Below, we refer to these points as the Landau zero points or modes. In the generic case, there is a split between zero energy points as shown in Fig. 1.

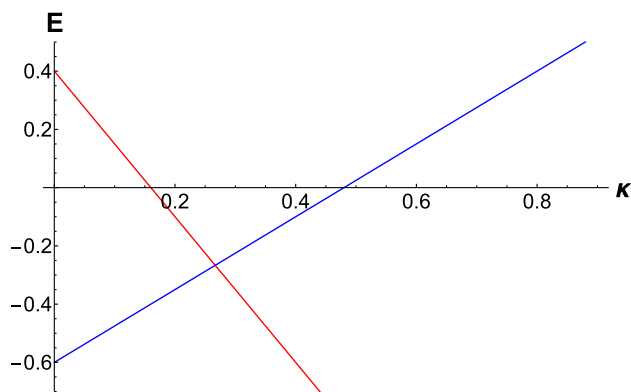


Fig. 1 The energy spectrum of the Hamiltonian Eq. (1) in the lowest Landau level as function of the magnetic field. The red line shows E_- and the blue line E_+ from Eq. (10). To emphasize the split between the Landau zero points, the model parameters are chosen as $(2T_-)^{-1} = -0.4$, $(2T_+)^{-1} = 0.8$, $\epsilon_0 = 0.1$, $\Delta_0 = 0.5$

For the material system of HgTe, the Landau zero point is degenerate, i.e., $E_+ = E_-$ and the corresponding critical field is roughly $B \sim 6\text{T}$ [7].

The distance between both critical fields on the field axis is given by

$$\Delta k_0 = |k_+ - k_-| = \left| \frac{\epsilon_0}{2T_+} - \frac{\epsilon_0}{2T_-} \right| + \left| \frac{\Delta_0}{2T_+} + \frac{\Delta_0}{2T_-} \right|. \tag{12}$$

This model is also relevant for the case of graphene [30–32]. The Hamiltonian describing the chemically neutral gapless graphene in the strong magnetic field follows from Eq. (1) by putting the diagonal elements to zero. Therefore, the eigenstates Eq. (8) are eigenstates of the graphene Hamiltonian too, i.e., the whole analysis is applicable to graphene as well. The only substantial difference is that for the gapless ($\Delta_0 = 0$) and chemically neutral ($\epsilon_0 = 0$) graphene, the energy of the the lowest Landau level is zero [30].

3 Single-particle propagator in the lowest Landau level

The advanced (+) or retarded (−) Green's function in the lowest Landau level can be calculated using the spectral representation

$$G_{r,r'}^\pm \sim \sum_{n=0}^\infty \varphi_n(r)\bar{\varphi}_n(r') \sum_{s=\pm} \frac{\mathcal{P}_s}{E - E_s \pm 0^+}, \tag{13}$$

where E_s are the eigenvalues of the Hamiltonian for each spin projection in the lowest Landau level Eq. (10) and the normalization will be fixed later. The projectors \mathcal{P}_\pm on the spin space

$$\mathcal{P}_+ = \begin{pmatrix} 0 & 0 & 0 & 0 \\ 0 & 1 & 0 & 0 \\ 0 & 0 & 0 & 0 \\ 0 & 0 & 0 & 0 \end{pmatrix} \quad \text{and} \quad \mathcal{P}_- = \begin{pmatrix} 0 & 0 & 0 & 0 \\ 0 & 0 & 0 & 0 \\ 0 & 0 & 1 & 0 \\ 0 & 0 & 0 & 0 \end{pmatrix} \quad (14)$$

are idempotent and orthogonal matrices with properties $\mathcal{P}_+\mathcal{P}_- = 0$, $\mathcal{P}_+\mathcal{P}_+ = \mathcal{P}_+$, $\mathcal{P}_-\mathcal{P}_- = \mathcal{P}_-$. The summation over all n yields

$$\begin{aligned} \sum_{n=0}^{\infty} \varphi_n(r)\bar{\varphi}_n(r') &= \frac{k^2}{\pi} e^{-\frac{k^2}{2}(|z|^2+|z'|^2)} \sum_{n=0}^{\infty} \frac{(k^2\bar{z}z')^n}{n!} \\ &= \frac{k^2}{\pi} e^{-\frac{k^2}{2}(|z|^2+|z'|^2-2\bar{z}z')}, \end{aligned} \quad (15)$$

which then gives for the Green’s function [9,33]

$$G_{r,r'}^{\pm}(E) = \frac{k^2}{2\pi} e^{-\frac{k^2}{2}(|z|^2+|z'|^2-2\bar{z}z')} \sum_{s=\pm} \frac{\mathcal{P}_s}{E - E_s \pm 0^+}. \quad (16)$$

Notably, the local Green’s function ($r = r'$) is a coordinate independent constant. The propagator is normalized this way to satisfy the usual sum rule

$$\mp \int_{-\infty}^{\infty} \frac{dE}{\pi} \text{Im} \text{tr} G_{r,r}^{\pm}(E) = \frac{k^2}{\pi} = \frac{eB}{h}, \quad (17)$$

where the trace operator acts only on the spin space. Eq. (17) gives the number of the elementary flux quanta $\phi_0 = h/e$ per unit volume. In the real-time representation, the Green’s function represents a simple collection of undamped harmonic functions with the period determined by the eigenenergies of the lowest Landau level modes

$$G_{r,r'}^{\pm}(t) = \mp i \frac{k^2}{2\pi} e^{-\frac{k^2}{2}(|z|^2+|z'|^2-2\bar{z}z')} \sum_{s=\pm} \mathcal{P}_s e^{\pm iE_s t}, \quad (18)$$

where the initial time is assumed to be at zero. The Green’s function is totally separable on the space–time.

For the case of chemically neutral gapless graphene, the Green’s function becomes particularly simple [33]:

$$G_{rr'}^{\pm}(E) = \frac{k^2}{2\pi} \frac{1}{E \pm i0^+} e^{-\frac{k^2}{2}(|r|^2+|r'|^2-2\bar{r}r')} [\mathcal{P}_+ + \mathcal{P}_-], \quad (19)$$

i.e., in the real-time representation it is just a step function $\theta(t)$.

4 Dressing of the single-particle propagator due to the disorder

The disorder is introduced in the form of the fluctuating chemical potential $v(r)$, which couples in the spin space to the unity matrix Σ_{00} , with the white noise correlator:

$$\langle v_r \rangle_g = 0, \quad \langle v_{r_1} v_{r_2} \rangle_g = g \delta_{r_1 r_2}. \quad (20)$$

The averaged propagator reads

$$\bar{G}_{r_1 r_2}^{\pm} = \langle [(G^{\pm})^{-1} + v \Sigma_{00}]_{r_1 r_2}^{-1} \rangle_g. \quad (21)$$

To perform the disorder average perturbatively, we expand the propagator in powers of v :

$$\begin{aligned} \bar{G}_{r_1 r_2}^{\pm} &= \langle G_{r_1 r_2}^{\pm} - G_{r_1 x_1}^{\pm} v_{x_1} G_{x_1 r_2}^{\pm} + G_{r_1 x_1}^{\pm} v_{x_1} G_{x_1 x_2}^{\pm} v_{x_2} G_{x_2 r_2}^{\pm} \\ &\quad - G_{r_1 x_1}^{\pm} v_{x_1} G_{x_1 x_2}^{\pm} v_{x_2} G_{x_2 x_3}^{\pm} v_{x_3} G_{x_3 r_2}^{\pm} \\ &\quad + G_{r_1 x_1}^{\pm} v_{x_1} G_{x_1 x_2}^{\pm} v_{x_2} G_{x_2 x_3}^{\pm} v_{x_3} G_{x_3 x_4}^{\pm} v_{x_4} G_{x_4 r_2}^{\pm} \\ &\quad - G_{r_1 x_1}^{\pm} v_{x_1} G_{x_1 x_2}^{\pm} v_{x_2} G_{x_2 x_3}^{\pm} v_{x_3} G_{x_3 x_4}^{\pm} v_{x_4} \\ &\quad \quad \quad G_{x_4 x_5}^{\pm} v_{x_5} G_{x_5 r_2}^{\pm} \dots \rangle_g, \end{aligned} \quad (22)$$

where the summation over multiple indices is understood. Because of Eq. (20) all terms with an odd number of potentials v vanish. The series then becomes

$$\begin{aligned} \bar{G}_{r_1 r_2}^{\pm} &= \langle G_{r_1 r_2}^{\pm} + G_{r_1 x_1}^{\pm} v_{x_1} G_{x_1 x_2}^{\pm} v_{x_2} G_{x_2 r_2}^{\pm} \\ &\quad + G_{r_1 x_1}^{\pm} v_{x_1} G_{x_1 x_2}^{\pm} v_{x_2} G_{x_2 x_3}^{\pm} v_{x_3} G_{x_3 x_4}^{\pm} v_{x_4} G_{x_4 r_2}^{\pm} \\ &\quad + G_{r_1 x_1}^{\pm} v_{x_1} G_{x_1 x_2}^{\pm} v_{x_2} G_{x_2 x_3}^{\pm} v_{x_3} G_{x_3 x_4}^{\pm} v_{x_4} \\ &\quad \quad \quad G_{x_4 x_5}^{\pm} v_{x_5} G_{x_5 x_6}^{\pm} v_{x_6} G_{x_6 r_2}^{\pm} \dots \rangle_g. \end{aligned} \quad (23)$$

The Green’s function Eq. (16) is spanned by the spin projectors \mathcal{P}_s . Therefore, only the disorder diagonal in the spin space is of importance. Besides the randomly fluctuating chemical potential considered here, these might include the randomly fluctuating gap, which couples to Σ_{03} , the random “chiral” chemical potential (Σ_{30}), or the random “chiral” mass (Σ_{33}). Each product of these matrices with \mathcal{P}_s projects them back onto \mathcal{P}_s again. Therefore, the perturbative series Eq. (23) does not depend on a particular disorder type and our analysis is generic and disorder type independent.

The exact Green’s function of disordered electrons in the lowest Landau level was obtained by Wegner in Ref. [9]. The constraint condition Eq. (17) changes it to, cf. Appendix 1.

$$\bar{G}_{rr'}^{\pm}(E) = \frac{k^2}{\pi} e^{-\frac{k^2}{2}(|r|^2+|r'|^2-2\bar{r}r')} \sum_{s=\pm} \mathcal{F}_s^{\pm}(E) \mathcal{P}_s, \quad (24)$$

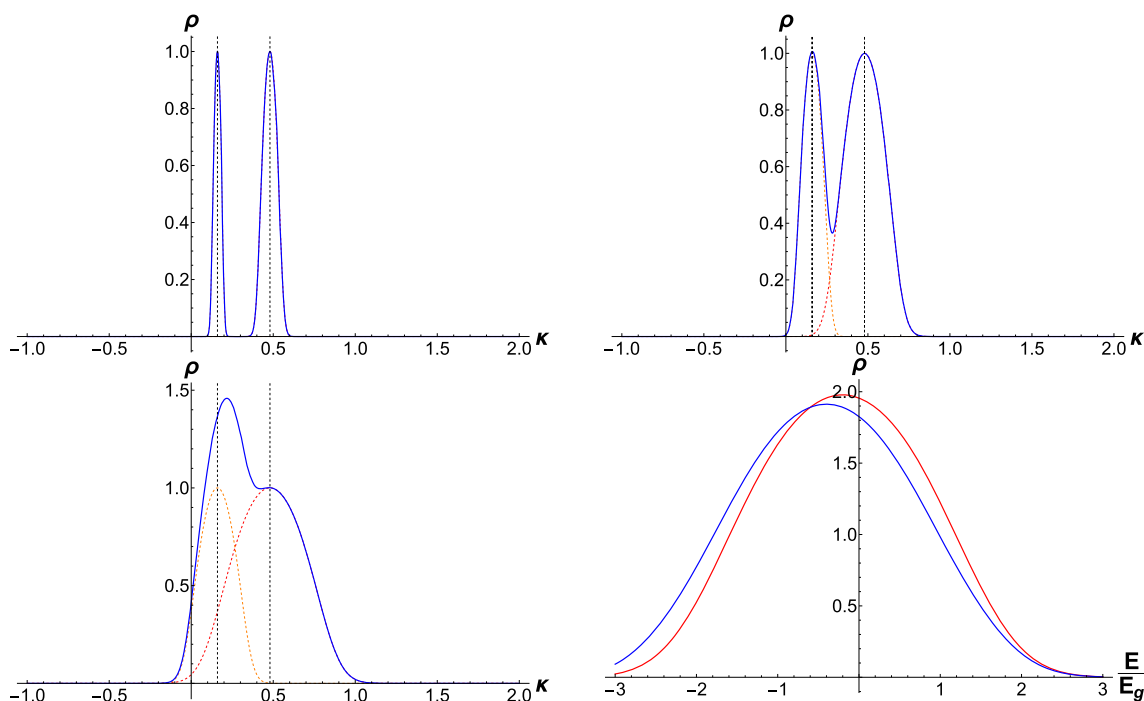


Fig. 2 Density of states (DOS) Eq. (29) calculated for the spectrum shown in Fig. 1 in units of $\frac{1}{\pi^{5/2}} \frac{k^2}{E_g}$. Top and bottom left: evolution of the DOS in the band center ($E = 0$) with increasing disorder strength as function of the magnetic field $k \sim \sqrt{B}$. Dashed lines emphasize the contributions to the net density of states from each Landau zero mode. The DOS is centered around the Landau zero points. Multiplying this function by the factor given in Eq. (60) gives the dc conductivity according to the Einstein relation Eq. (37). Bottom right: DOS as function of the dimensionless energy E/E_g for the magnetic fields adjusted to each of the Landau zero points in Fig. 1. Here, the color scheme of Fig. 1 is preserved

where the frequency-dependent part

$$\mathcal{F}_s^\pm(E) = \eta_s(E) \mp i\rho_s(E) \tag{25}$$

has the following explicit expressions for the real

$$\eta_s(E) = \frac{1}{E_g} \left(\frac{2}{\pi} \frac{e^{\nu_s^2} \int_0^{\nu_s} dt e^{t^2}}{1 + \left(\frac{2}{\sqrt{\pi}} \int_0^{\nu_s} dt e^{t^2} \right)^2} - \nu_s \right) \tag{26}$$

and imaginary part [10, 11]

$$\rho_s(E) = \frac{1}{\sqrt{\pi} E_g} \frac{e^{\nu_s^2}}{1 + \left(\frac{2}{\sqrt{\pi}} \int_0^{\nu_s} dt e^{t^2} \right)^2}. \tag{27}$$

They depend on the dimensionless energy

$$\nu_s = \frac{E - E_s}{E_g}, \text{ where } E_g^2 = \frac{gk^2}{4\pi}. \tag{28}$$

In the chosen units, the disorder-related energy E_g is a dimensionless quantity. It represents essentially the ratio of two relevant lengths $E_g \sim l_\lambda/\ell$: the magnetic

length $\ell \sim 1/k$ and the disorder-related length $l_\lambda \sim \sqrt{g}$. The collective density of states

$$\begin{aligned} \rho(E) &= \mp \frac{1}{\pi} \text{Im tr} G_{rr}^\pm(E) \\ &= \frac{1}{\pi^{5/2}} \frac{k^2}{E_g} \sum_{s=\pm} \frac{e^{\nu_s^2}}{1 + \left(\frac{2}{\sqrt{\pi}} \int_0^{\nu_s} dt e^{t^2} \right)^2} \end{aligned} \tag{29}$$

is correctly normalized in accordance with Eq. (17). Fig. 2 shows Eq. (29) for spectrum from Fig. 1. For weak disorder strength, the density of states appears in the form of two sharp peaks placed symmetrically around the Landau zeros. It is plotted in units of $\frac{1}{\pi^{5/2}} \frac{k^2}{E_g} \sim (\ell l_\lambda)^{-1}$, with ℓl_λ being the parametric volume constructed from the two specific lengths of the model. The peaks become boarder with increasing disorder strength and overlap with each other until they merge to a single structure.

Performing the Fourier transformation, we obtain the Wegner’s propagator in the time representation. It comprises two parts, one periodically oscillating in time and the second localized in the time with the maximum at zero time, cf. Appendix 1:

$$\mathcal{F}_s^\pm(t) = \mp \frac{i}{2} e^{\pm i E_s t} \Omega(E_g t). \tag{30}$$

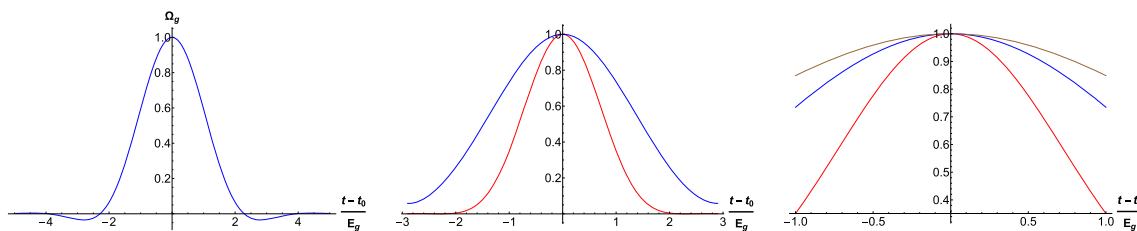


Fig. 3 Left: The shape of the function $\Omega(E_g t)$ from Eq. (C15) determined to the order $(E_g t)^{60}$. Middle: the second time convolution of the Wegner’s function Eq. (40) (blue line) in comparison to $\Omega^2(E_g t)$ (red line). Right: same distributions as in the middle panel plus the fourth time convolution (brown line) Eq. (42) for small times. All curves are normalized to 1 at their maxima in the respective units. The higher the order of the convolution, the broader is its distribution

The real part of the Wegner’s propagator is antisymmetric in time, while the imaginary part is symmetric. Notably, the period of oscillations is still determined only by energies of the clean system, while the temporarily localized part $\Omega(E_g t)$ depends only on the disorder-related energy E_g . It is shown in Fig. 3 and represents a smooth and strongly damped oscillating function symmetrically placed around $t = 0$. The series of $\Omega(E_g t)$ contains only even powers of $E_g t$ and goes for small times as $\Omega(E_g t) \sim 1 - \text{const} \cdot t^2$.

5 Mean-squared displacement of the disordered system

The access to the diffusion goes via the mean-squared displacement

$$\langle r_\mu^2(t) \rangle = \frac{\text{tr} \sum_r r_\mu^2 P_{r0}(t)}{\text{tr} \sum_r P_{r0}(t)}, \tag{31}$$

where r_μ is the position operator and $P_{rr'}(t)$ is the return probability density defined as

$$P_{rr'}(t) = \int \frac{dE}{2\pi} e^{-iEt} P_{rr'}(E), \tag{32}$$

where

$$P_{rr'}(E) = \langle G_{rr'}^+(E) G_{r'r}^-(E) \rangle_g \tag{33}$$

is the disorder averaged two-particle propagator. The large-time asymptotics of the mean-squared displacement is expected to be of the form [23–25]

$$\lim_{t \rightarrow \infty} \langle r_\mu^2(t) \rangle \rightarrow 2Dt^{1+\alpha} + \text{const}, \tag{34}$$

where D is the diffusion coefficient and the exponent α is referred to as the anomalous dimension and can be either positive (superdiffusion) or negative (subdiffusion) [23]. For instance, for the ordinary diffusion $\alpha = 0$ with $P_{r0} \sim \exp[r^2/Dt]/Dt$, which can be easily verified

by evaluating Eq. (31) [26]. In the linear regime, the relation between the mean-squared displacement and diffusion is established via

$$\left. \frac{d}{dt} \langle r_\mu^2(t) \rangle \right|_{t=0} = 2D. \tag{35}$$

To start with, we evaluate Eq. (31) for the case of clean system. Because the real-time representation of the Green’s function of clean system Eq. (18) is totally separable into the spatial and temporal parts, the same is also valid for the return probability density $P_{r,r'}(t) = R(r, r')T(t)$. Hence, the time-dependent parts cancel each other in Eq. (31) exactly and we are left with a simple result

$$\langle r_\mu^2(t) \rangle = \frac{\ell^2}{2}, \tag{36}$$

where we use explicitly the magnetic length defined in Eq. (4) and the factor 1/2 is attributed to the angular average. The result is transparent: it gives the expected position of an electron to be a circle with radius ℓ around the position of the flux tube piercing the sample at the origin of the coordinates.

Our task is to determine the diffusion coefficient of the disordered system through the direct evaluation of Eq. (31), to compute the conductivity from the Einstein relation

$$\sigma = \frac{e^2}{\hbar} D \rho(E), \tag{37}$$

where $\rho(E)$ is the density of states discussed in the previous paragraph.

A rigorous evaluation of the full perturbative series for the two-particle propagator $\langle G_{r,0}^+ G_{0,r}^- \rangle_g$ along the lines of Wegner’s calculations for the single-particle propagator is principally impossible. The reason for this is the spatial decoherence in higher orders of perturbative expansion, cf. Appendix 1: wWhile the disorder does not affect the spatial dependence of the single-particle propagator, it does so for the two-particle propagator. Thus, we need to consider the spatial averages. We evaluate both expressions from the numerator and denominator of Eq. (31) perturbatively. Evaluation of

all perturbative diagrams to order g^3 yields for the numerator of Eq. (31)

$$\begin{aligned} \text{tr} \sum_r r_\mu^2 P_{r0}(E) &= \frac{1}{4\pi} \frac{1}{E_g^2} \sum_{s=\pm} (2X_s)^2 \\ &\left[\frac{1}{2} + (2X_s)^2 + 2(2X_s)^4 + \frac{167}{36} (2X_s)^6 + \dots \right. \\ &+ \left(\frac{3}{4} (2X_s)^4 + \frac{343}{72} (2X_s)^6 + \dots \right) \cos 2\phi_s \\ &\left. + \left(\frac{139}{72} (2X_s)^6 + \dots \right) \cos 4\phi_s + \dots \right], \end{aligned} \quad (38)$$

where $X_s^2(E) = E_g^2[\eta_s^2(E) + \rho_s^2(E)]$ and $\phi_s(E) = \arctan \left[\frac{\rho_s(E)}{\eta_s(E)} \right]$. According to Eqs. (26) and (27), $X_s^2(E)$ and $\phi_s(E)$ are dimensionless functions of the argument $\nu_s = (E - E_s)/E_g$. The analogous computation for the denominator of Eq. (31) yields

$$\begin{aligned} \text{tr} \sum_r P_{r0}(E) &= \frac{k^2}{4\pi} \frac{1}{E_g^2} \sum_{s=\pm} (2X_s)^2 \\ &\left[1 + (2X_s)^2 + \frac{3}{2} (2X_s)^4 + \frac{13}{4} (2X_s)^6 + \dots \right. \\ &+ \left((2X_s)^4 + \frac{9}{2} (2X_s)^6 + \dots \right) \cos 2\phi_s \\ &\left. + \left(\frac{5}{2} (2X_s)^6 + \dots \right) \cos 4\phi_s + \dots \right]. \end{aligned} \quad (39)$$

Technical details of the evaluation and results for each individual diagram are summarized in Appendices 1 and 1.

At first, one can try to Fourier transform each individual term in both series. Essentially, the Fourier transformation of Eqs. (38) and (39) are given in terms of the even time convolutions of the temporal part of the Wegner’s propagator Eq. (30)

$$\int_{-\infty}^{\infty} \frac{dE}{\pi} e^{iEt} X_s^2(E) \sim \int_{-\infty}^{\infty} d\tau \Omega(E_g\tau)\Omega(E_g[\tau + t]), \quad (40)$$

$$\begin{aligned} \int_{-\infty}^{\infty} \frac{dE}{\pi} e^{iEt} X_s^4(E) &\sim \int_{-\infty}^{\infty} d\tau_1 \int_{-\infty}^{\infty} d\tau_2 \\ &\int_{-\infty}^{\infty} d\tau_3 \Omega(E_g\tau_1)\Omega(E_g[\tau_1 + \tau_3]) \\ &\quad (41) \end{aligned}$$

$$\times \Omega(E_g\tau_2)\Omega(E_g[\tau_2 + \tau_3 + t]), \quad (42)$$

and so on. In practice though, this can be done to an extent only. To the best of our knowledge, the function $\Omega(E_g\tau)$ itself is not tabulated and its polynomial series

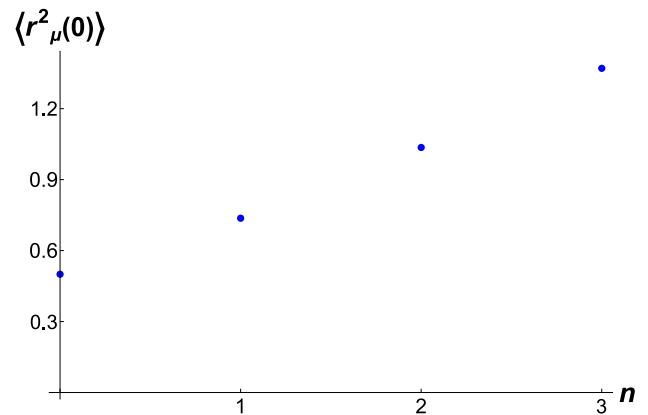


Fig. 4 The initial mean-squared displacement $\langle r_\mu^2(0) \rangle$ Eq. (44) in units of k^{-2} evaluated to different order ($n = 0, 1, 2, 3$) of perturbative expansion

has to be truncated at some order. For practical calculations, we use the polynomial with 31 terms (order $(E_g t)^{60}$), which is sufficient to determine the second convolution Eq. (40) only to the order $(E_g t)^{20}$, and the fourth convolution Eq. (42) only to the order $(E_g t)^6$, cf. Fig. 3. The convolutions have a typical bell-curve shape. This result suffices to recognize that every higher-order convolution is broader and therefore, the large time asymptotics of the mean-squared displacement is determined by the higher-order terms in the series Eqs. (38) and (39). Another aspect is that since the Wegner’s propagator is uniquely separable in temporal and spatial variables, the large-time asymptotics of the numerator and denominator of Eq. (31) differ only in amplitudes, but not in functional behavior. Hence, we can expect that for large times the mean-squared displacement approaches a time-independent constant, similarly to the case of the clean system Eq. (36) and the time evolution ends up in a stationary state. In this state, all electrons are again localized at fixed orbits and no currents can flow through the sample. If there be a diffusion in the system, i.e., the regime linear in time with a positive slope, then it can only emerge due to the superposition of all convolutions at intermediate time scales.

To give these general arguments a more firm footing, we propose a resummation procedure leaned on the general idea of the renormalization group. We start with the considerations of the mean-squared displacement at time zero

$$\langle r_\mu^2(0) \rangle = \frac{\text{tr} \int_{-\infty}^{\infty} dE \sum_r r_\mu^2 P_{r0}(E)}{\text{tr} \int_{-\infty}^{\infty} dE \sum_r P_{r0}(E)}. \quad (43)$$

Changing to the integration over ν_s , we then have

$$k^2 \langle r_\mu^2(0) \rangle = \frac{\sum_{s=\pm} \int_{-\infty}^{\infty} d\nu_s f^{(2)}(\nu_s)}{\sum_{s=\pm} \int_{-\infty}^{\infty} d\nu_s f^{(0)}(\nu_s)} = \frac{\langle f^{(2)} \rangle}{\langle f^{(0)} \rangle}, \quad (44)$$

where

$$\begin{aligned} \langle f^{(2)} \rangle &= \text{tr} \int_{-\infty}^{\infty} d\nu_s \sum_{r,s=\pm} r_\mu^2 P_{r0}(\nu_s), \\ \text{and } \langle f^{(0)} \rangle &= \text{tr} \int_{-\infty}^{\infty} d\nu_s \sum_{r,s=\pm} P_{r0}(\nu_s). \end{aligned} \quad (45)$$

Each of both spin projections contribute equally in $t = 0$ limit and we can skip the summation over s . In Fig. 4 we plot the right hand side of Eq. (44) evaluated for the increasing order n of perturbative expansion.

With larger n the statical mean-squared displacement approaches a linear asymptotics as function of n . Among all possible diagrammatic channels, there is a unique channel which suffices this property. This includes all diagrams of the so-called ladder channel, cf. Appendix 1. Assembling all ladder diagrams yields the asymptotics of the two-particle propagator in the form of an infinite series

$$P_{r0}^{\text{lad}}(E) \approx \frac{1}{4E_g^2} \left(\frac{k^2}{\pi} \right)^2 \sum_{s=\pm} \sum_{n=1}^{\infty} \frac{(2X_s)^{2n}}{n} \exp \left[-\frac{k^2 r^2}{n} \right]. \quad (46)$$

This expression gives rise to the series element of the denominator of Eq. (44) in the form

$$\langle f_n^{(0)} \rangle^{\text{lad}} = \frac{k^2}{4\pi E_g^2} \sum_{s=\pm} \int_{-\infty}^{\infty} d\nu (2X_s)^{2n}, \quad (47)$$

and for the numerator

$$\langle f_n^{(2)} \rangle^{\text{lad}} = \frac{1}{4\pi E_g^2} \sum_{s=\pm} \int_{-\infty}^{\infty} d\nu \frac{n}{2} (2X_s)^{2n}. \quad (48)$$

Because the argument $2X_s$ is larger than 1 at its maximum, the series do not converge. Hence, at every finite expansion order, the behavior of both numerator and denominator of the mean-squared displacement is dominated by the respective last terms in the series, which then cancel within the formula for $\langle r_\mu^2(0) \rangle$ Eq. (43). In this way, the linear dependence of $\langle r_\mu^2(0) \rangle \sim n/2$ visible in Fig. 4 emerges. All remaining channels exhibit either slower logarithmic grow or decay with increasing n , which allows to neglect them.

6 Equation of motion for the mean-squared displacement

To arrive at the equation of motion for the mean-squared displacement, we assume that it is possible to determine the perturbative series up to a large order N . In this limit, using of the approximate formulas Eqs. (47) and (48) is justified. If necessary, the limit $N \rightarrow \infty$ can be carried out at the end of the calculations. We write Eq. (44) as

$$k^2 \langle r_\mu^2(0) \rangle = \frac{\langle f_0^{(2)} \rangle + \langle \delta f^{(2)} \rangle}{\langle f_0^{(0)} \rangle + \langle \delta f^{(0)} \rangle}. \quad (49)$$

In Eq. (49), $\langle f_0^{(i)} \rangle$ includes all terms of the respective series with the exception of the N th. The latter are contained in the fluctuation terms $\langle \delta f^{(i)} \rangle$ and are treated as the generators of the time evolution of $\langle r_\mu^2 \rangle$ at small positive/negative times Δt . After some algebra presented in Appendix 1, we obtain a self-consistent equation of motion for $\langle r_\mu^2(t) \rangle$ in the form of the second-order ordinary differential equation

$$k^2 \frac{\partial^2}{\partial t^2} \langle r_\mu^2(t) \rangle = -E_g^2 I_N \left[\frac{N}{2} - k^2 \langle r_\mu^2(t) \rangle \right]. \quad (50)$$

The integral I_N in the expression for the time-dependent diffusion coefficient is defined as

$$\begin{aligned} I_N &= \frac{1}{\langle f^{(0)} \rangle} \sum_{s=\pm} \int_{-\infty}^{\infty} d\nu_s \nu_s^2 (2X_s)^{2N} \\ &\approx \frac{\int_{-\infty}^{\infty} d\nu \nu^2 X^{2N}(\nu)}{\int_{-\infty}^{\infty} d\nu X^{2N}(\nu)}, \end{aligned} \quad (51)$$

where we approximated $\langle f^{(0)} \rangle$ by the largest power in the series. Integral I_N shows a very slow decay for large N , cf. Fig. 5, and seems to approach a finite limit for infinitely large N . Numerical routines struggle to compute it much beyond $N = 600$ and it remains an open question whether the $N \rightarrow \infty$ bound exists. In turn, the product NI_N grows very slowly, which can also be interpreted as approaching a finite value in the limit $N \rightarrow \infty$.

The large-time asymptotics ($t \gg t_c$, t_c being some crossover time far in the past, which can be chosen as zero) is given by the solution of the self-consistent equation

$$\langle r_\mu^2(t) \rangle \approx \frac{N}{2} \ell^2 + \ell^2 \mathcal{C} \exp \left[-\frac{t}{\tau} \right], \quad (52)$$

where we introduced the scattering time as

$$\tau \approx \frac{1}{\sqrt{I_N} E_g}. \quad (53)$$

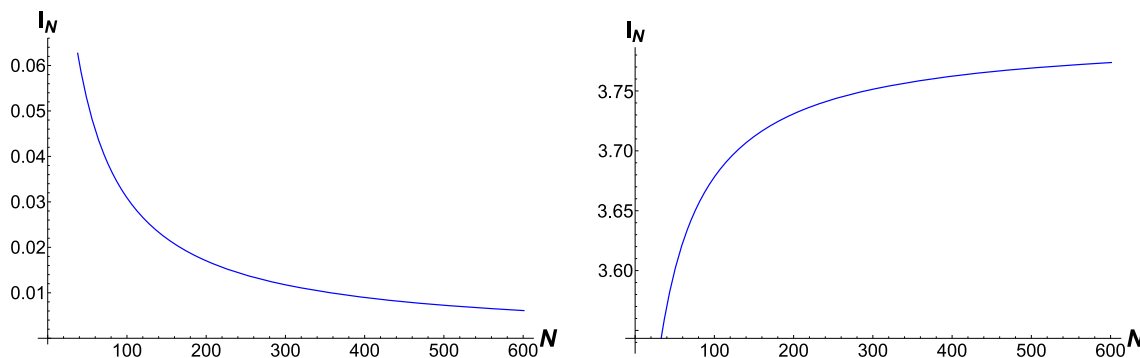


Fig. 5 Integral I_N Eq. (51) (left) and product NI_N (right)

In the limit $t \rightarrow \infty$, the mean-squared displacement approaches its upper bound

$$\lim_{t \rightarrow \infty} \langle r_\mu^2(t) \rangle \rightarrow \frac{N}{2} \ell^2, \tag{54}$$

which for $N \rightarrow \infty$ lies in the infinity and is therefore never reached. Hence, it can be only approached from below, which requires \mathcal{C} to be negative. If $\sqrt{I_N}$ is small, then τ is large and the regime with linear time dependence should be broad. The diffusion coefficient is then obtained from

$$\left. \frac{\partial}{\partial t} \langle r_\mu^2(t) \rangle \right|_{t=t_c} = |\mathcal{C}| \frac{\ell^2}{\tau}. \tag{55}$$

Formally, $|\mathcal{C}|$ should follow from the initial condition at $t = t_c$, but for this we need to know $\langle r_\mu^2(t_c) \rangle$, which lies far in the past and therefore forgotten. To be a physical quantity, we demand for D an invariance with respect to N . This is similar to the version of the renormalization group typically used in the high energy physics. This implies

$$\frac{\partial}{\partial N} (\sqrt{I_N} |\mathcal{C}|) = 0, \tag{56}$$

from where then follows

$$\sqrt{I_N} |\mathcal{C}| = \text{const.} \tag{57}$$

Even though this constrain might appear not entirely transparent, it has a natural analogy in the case of disordered electron gas without magnetic field. Here, the diffusion coefficient is determined from the self-consistent Born approximation and appears unchanged in the partial series, e.g., Cooperon or diffuson [38, 39]. Comparison with Eq. (34) suggests this constant to be 2. Then the physical diffusion coefficient becomes

$$D \approx \frac{E_g}{k^2} \sim \ell l_\lambda, \tag{58}$$

i.e., it is proportional to the parametric volume of the model.

Inserting the density of states from Eq. (29) and the diffusion coefficient Eq. (58) into the Einstein relation Eq. (37) yields the conductivity. The system is conducting within a parametric window located around each of the Landau zeros. The width of the conducting window is determined by the parameters of the microscopic model and by the disorder. The transition $g \rightarrow 0$ is smooth and the conductivity degenerates to two sharp peaks at the Landau zeros. With increasing disorder, the peaks becomes broader and merge at some point to an amorphous structure. Simultaneously the amplitude becomes smaller, signaling the suppression of the conductivity in the strong disorder limit.

We can compute the conductivity at an arbitrary Landau zero point. For weak disorder, the contribution from the other mode is negligible and we get for the density of states

$$\rho^{\text{LZ}} \approx \frac{1}{\pi^{5/2}} \frac{k^2}{E_g}. \tag{59}$$

Using the units of e^2/h instead of e^2/h adds an extra factor of 2π , i.e.,

$$\sigma^{\text{LZ}} \approx \frac{2\pi}{\pi^{5/2}} \frac{e^2}{h} \approx 0.36 \frac{e^2}{h}. \tag{60}$$

Numerically, it is close to the dc limit of the optical conductivity of a single Dirac electron (which also has a zero energy point in the spectrum) in clean and even weakly disordered systems, which depending on the way it is calculated is either $\frac{e^2}{\pi h} \approx 0.32 \frac{e^2}{h}$ or $\frac{\pi e^2}{8h} \approx 0.39 \frac{e^2}{h}$ [37, 40–44]. If compared to the established value evaluated for conventional electron gas with the spectrum without zero points, then the Padé-Borel resummation [11, 12, 27] gives the value $0.46 \frac{e^2}{h}$, while the numerical value of Ref. [35] is $0.5 \frac{e^2}{h}$ within a statistical uncertainty of 10%. However, we are not aware of any further results for the static conductivity at the Landau zero points.

7 Discussions

The electronic transport properties of disordered electronic systems in strong magnetic fields represents a technically very demanding problem, which evades a conclusive solution even despite several decades of active research. In the past, there have been impressive breakthroughs, though. At the single-particle level, the problem has been effectively resolved by Ando [8] and Wegner [9]. The latter work provided an exact expression for the single-particle propagator. The resulting Green's function does not reveal any singularities and describes a state of the matter without pronounced resonances and consequently without clearly defined quasi-particles.

On the technical side, the difficulties aggregate if one goes beyond the single-particle picture and considers processes involving two or more particles. While the single-particle propagator retains its form in the position space in every order of perturbative expansion, which suggests a kind of invariance under the operation of perturbative expansion, the two-particle propagator does not show up this property. Instead, the disorder washes out the expansion series in the position space, making higher-order terms broader in comparison to the clean system. This is the reason why the Wegner's technique cannot be applied to the two-particle propagator with the same success. From studying previous works available to us, it is not clear whether this simple fact has been realized so far.

In our work, we perform the perturbative expansion in powers of disorder strength and classify all scattering processes into two main groups. The first group are those which dress the single-particle propagators. To order g^3 , all of these diagrams are shown in Fig. 7. They are absorbed into the fully dressed single-particle propagators, for which exact results are known [9,10]. Secondly, there are processes which cannot be accounted for at the single-particle level. They are represented by loop diagrams, which involve at least one scattering process between the advanced and retarded sides. To order g^3 all of them are shown in Fig. 6. We take all diagrams to third order into account, without truncating the perturbative series. Ideally, one would compute all diagrams in all orders of expansion. The number of diagrams grows rapidly with increasing order of expansion though, while the computational effort for the evaluation of every individual diagram increases considerably. However, it is possible to extract the diagrammatic channel which dominates the large-scale behavior of the two-particle propagator. Still, due to the absence of a small expansion parameter, the obtained series do not show any sign of convergence [13].

Our main intention is to calculate the transport coefficients, in particular the static conductivity. Because the series diverge, a naive use of the Kubo formula fails. Therefore we approach the conductivity via the Einstein relation, which requires the knowledge of the density of states and of the diffusion coefficient. While the former is known from the Wegner's solution, the

latter is not. We acquire it from the mean-squared displacement, which at large times should be proportional to the diffusion coefficient. For infinite times, the mean-squared displacement approaches an infinite time-independent value. The processes linear in time emerge at the timescales determined by the combined action of disorder and magnetic field. The former being weak and the latter strong puts this characteristic time to considerable absolute values, which can indeed appear as the large-time limit in an experiment. Whatever happens at larger times can evoke an impression of the onset subdiffusion. The infinite times asymptotics might be inaccessible in realistic measurements. With this, we can compute the conductivity from the Einstein relation with the extracted diffusion coefficient.

For discussions of a concrete physical system, we consider the BZH-Hamiltonian [29]. Its lowest Landau level energy spectrum has two modes, corresponding to the two particle species related to each other by the time-reversal symmetry. Both modes exhibit zero energy points at critical magnetic fields, the so-called Landau zero modes. It is possible to lift the degeneracy of the Landau zero points parametrically, i.e., to move them apart from each other on the magnetic field axis. The analytical expressions for the conductivity adopted for this case suggest that the system becomes metallic in the parametric window around the Landau zeros. The weaker the disorder, the narrower is the metallic window. This picture appears rather intuitive and hopefully likely to be confirmed experimentally with a modest effort. Adjusting the magnetic field exactly to the zero Landau energy gives for the conductivity a universal value $\sim 0.36e^2/h$, which is surprisingly close to the established results for the conductivity of the disordered Dirac electrons without magnetic fields and also have zero energy points in the spectrum.

The most obvious avenue leading beyond the scope of the present work is the challenge of reconciling the Einstein relation with the Kubo–Greenwood formalism [34,36,37,44]. In the Kubo–Greenwood formalism, the computation of the conductivity requires the knowledge of the two-particle propagators as well. However, usually the Kubo–Greenwood formula does not involve any normalization and the issue of series convergence becomes much more urgent. Curiously though, the static conductivity of the clean system can be straightforwardly evaluated from the Kubo–Greenwood formula, giving the value of $e^2/2h$ for each Landau mode. At the first superficial glance, once the disorder is brought into the system this conductivity is destroyed. Another possible direction is an extension to the higher Landau levels. These problems are left for the future activities.

Acknowledgements A.S. acknowledges the support by the grants of the Julian Schwinger Foundation for Physics Research and expresses his gratitude to Prof. C. Weber for hospitality during the later phase of manuscript preparation. The work was concluded at IMDEA Nanotecnologia Madrid with the support from the personal research grant

(A.S.) PCI2021-122057-2B (MSCA IF EF-ST 2020) of the Agencia Estatal de Investigacion, Spain.

Funding Open Access funding enabled and organized by Projekt DEAL.

Data availability statement This manuscript has no associated data or the data will not be deposited. [Authors' comment: This is a theoretical study which has no experimental data.]

Open Access This article is licensed under a Creative Commons Attribution 4.0 International License, which permits use, sharing, adaptation, distribution and reproduction in any medium or format, as long as you give appropriate credit to the original author(s) and the source, provide a link to the Creative Commons licence, and indicate if changes were made. The images or other third party material in this article are included in the article's Creative Commons licence, unless indicated otherwise in a credit line to the material. If material is not included in the article's Creative Commons licence and your intended use is not permitted by statutory regulation or exceeds the permitted use, you will need to obtain permission directly from the copyright holder. To view a copy of this licence, visit <http://creativecommons.org/licenses/by/4.0/>.

Appendix A: BHZ-Hamiltonian in explicit form

Without magnetic field, the BHZ-Hamiltonian Eq. (1) reads:

$$H = \begin{pmatrix} -T_- \nabla_+ \nabla_- - \epsilon_0 + \Delta_0 & -i v \nabla_- & 0 & 0 \\ -i v \nabla_+ & -T_+ \nabla_+ \nabla_- - \epsilon_0 - \Delta_0 & 0 & 0 \\ 0 & 0 & -T_- \nabla_+ \nabla_- - \epsilon_0 + \Delta_0 & -i v \nabla_+ \\ 0 & 0 & -i v \nabla_- & -T_+ \nabla_+ \nabla_- - \epsilon_0 - \Delta_0 \end{pmatrix}. \tag{A1}$$

All quantities are explained in Sect. 2. The model does not presume any coupling or scattering mechanisms between spin projections (or valleys), which would appear in the off-diagonal blocs. To introduce the magnetic field, we replace $\nabla_- \rightarrow 2\partial_z + k^2 \bar{z} = A$, $\nabla_+ \rightarrow 2\partial_{\bar{z}} - k^2 z = A^\dagger$, and $\nabla_+ \nabla_- \rightarrow (2\partial_{\bar{z}} - k^2 z)(2\partial_z + k^2 \bar{z}) - 2k = A^\dagger A - 2k$.

Appendix B: Technical preliminary

In Sect. 5 we emphasize that, while the position dependence of the single-particle propagator $G_{rr'}^\pm$ of an electron in the lowest Landau level is preserved in every order of perturbative expansion, this is not so for the two-particle propagator $G_{rr'}^+, G_{r'r}^-$. We demonstrate this by evaluating the respective leading order terms. The calculations are easy to perform using the following integration formula:

$$\frac{1}{\pi} \int d\bar{x} dx e^{-[c\bar{x}x - a\bar{y}x - b\bar{x}z]} = \frac{1}{c} \exp \left[\frac{ab}{c} \bar{y}z \right], \tag{B1}$$

$(a, b, c) > 0$.

After performing the disorder average in the lowest order of the single-particle propagator, we have

$$\begin{aligned} \langle G_{rx}^\pm v_x G_{xy}^\pm v_y G_{yr'}^\pm \rangle_g &= g \sum_{xy} \delta_{xy} G_{rx}^\pm G_{xy}^\pm G_{yr'}^\pm \\ &= g \sum_x G_{rx}^\pm G_{xx}^\pm G_{xr'}^\pm. \end{aligned} \tag{B2}$$

The local propagator G_{xx}^\pm is a position-independent constant. Because of the idempotence of projectors, the product of Green's functions is separable in the spin space (for the sake of simplicity we skip below the convergence factor $\pm i0^+$, unless the opposite is necessary):

$$\begin{aligned} g \sum_x G_{rx}^\pm G_{xx}^\pm G_{xr'}^\pm &= g \left(\frac{k^2}{2\pi} \right)^3 \sum_{s=\pm} \frac{\mathcal{P}_s}{[E - E_s]^3} \\ &\int d\bar{x} dx e^{-\frac{k^2}{2}(|r|^2 + |x|^2 - 2\bar{r}x)} e^{-\frac{k^2}{2}(|x|^2 + |r'|^2 - 2\bar{x}r')}. \end{aligned} \tag{B3}$$

We evaluate the integral as follows:

$$\begin{aligned} &\int d\bar{x} dx e^{-\frac{k^2}{2}(|r|^2 + |x|^2 - 2\bar{r}x)} e^{-\frac{k^2}{2}(|x|^2 + |r'|^2 - 2\bar{x}r')} \\ &= e^{-\frac{k^2}{2}(|r|^2 + |r'|^2)} \int d\bar{x} dx e^{-k^2(\bar{x}x - \bar{r}x - \bar{x}r')} \\ &= e^{-\frac{k^2}{2}(|r|^2 + |r'|^2 - 2\bar{r}r')}, \end{aligned} \tag{B4}$$

where in the last line we used the formula Eq. (B1). Putting all terms together we get

$$\begin{aligned} g \sum_x G_{rx} G_{xx} G_{xr'} &= \frac{g}{2} \left(\frac{k^2}{2\pi} \right)^2 e^{-\frac{k^2}{2}(|r|^2 + |r'|^2 - 2\bar{r}r')} \\ &\sum_{s=\pm} \frac{\mathcal{P}_s}{[E - E_s]^3}. \end{aligned} \tag{B5}$$

Indeed, the spatial part of this expression is the same as that of the Green's function of the clean system. This property can be traced back in every order of perturbative expansion, irrespective of the diagram's topology. This means that the disorder does not affect the coherence of the single-particle Green's function and, therefore, the series can be summed up exactly [9, 10].

To illustrate the effect of the disorder on the two-particle propagator, we start with the expression of the clean system:

$$\begin{aligned} G_{rr'}^+ G_{r'r}^- &= \left(\frac{k^2}{2\pi} \right)^2 e^{-k^2(\bar{r}-\bar{r}')(r-r')} \\ &\sum_{s=\pm} \frac{\mathcal{P}_s}{(E - E_s - i0^+)(E - E_s + i0^+)}. \end{aligned} \tag{B6}$$

Table 1 Gaussian exponents χ_i of all perturbative processes contributing to the two-particle Green’s function shown in Fig. 6

No.	Diagram	Exponent	No.	Diagram	Exponent	No.	Diagram	Exponent
1		1	6		3/4	12		2/3
2		1/2	7		3/4	13		1/2
3		1/3	8		2/3	14		1/4
4		1/2	9		3/5	15		1/2
5		2/3	10		3/5	16		1/3
			11		2/5	17		1/2

The two-particle propagator is a real-valued quantity and decays exponentially in the position space with the Gaussian exponent 1. The leading order perturbative vertex correction reads

$$g \sum_x G_{rx}^+ G_{xr'}^+ G_{r'x}^- G_{xr}^- = g \left(\frac{k^2}{2\pi}\right)^4 \sum_{s=\pm} \frac{\mathcal{P}_s}{(E - E_s - i0^+)^2 (E - E_s + i0^+)^2} \quad (B7)$$

$$\times \int d\bar{x} dx e^{-k^2(\bar{r}-\bar{x})(r-x)} e^{-k^2(\bar{x}-\bar{r}')(x-r')}. \quad (B8)$$

At first, the integral can be rewritten as

$$\int d\bar{x} dx e^{-k^2(\bar{r}-\bar{x})(r-x)} e^{-k^2(\bar{x}-\bar{r}')(x-r')} = e^{-k^2(|r|^2+|r'|^2)} \int d\bar{x} dx e^{-k^2[2|x|^2-\bar{x}(r+r')-(\bar{r}+\bar{r}')x]}, \quad (B9)$$

which gives with the help of Eq. (B1)

$$g \sum_x G_{rx}^+ G_{xr'}^+ G_{r'x}^- G_{xr}^- = \frac{g}{2^2} \left(\frac{k^2}{2\pi}\right)^3 e^{-\frac{k^2}{2}(\bar{r}-\bar{r}')(r-r')} \sum_{s=\pm} \frac{\mathcal{P}_s}{(E - E_s - i0^+)^2 (E - E_s + i0^+)^2}. \quad (B10)$$

Comparing this with Eq. (B6), we recognize the different Gaussian exponent 1/2, i.e., the spatial part of the first correction is broader than that of the clean system. This effect takes place in all orders, but differently for topologically different diagrammatic channels, i.e., the coherence of the two-particle propagator is violated by the disorder. This is the ultimate reason why the adoption of the Wegner’s technique to the two-particle propagator is difficult. Table 1 shows the Gaussian exponents for each diagram from Fig. 6. They reveal certain patterns for particular diagrammatic channels. For instance, one recognizes that the large-scale behavior in every order of perturbative expansion is dominated by the diagrams belonging to the so-called ladder channel. Those are the diagrams no. 1, 2, 3 and 4. The dominant oscillating channel is represented by the diagrams no. 5, 7, etc., which we call the menora diagrammatic

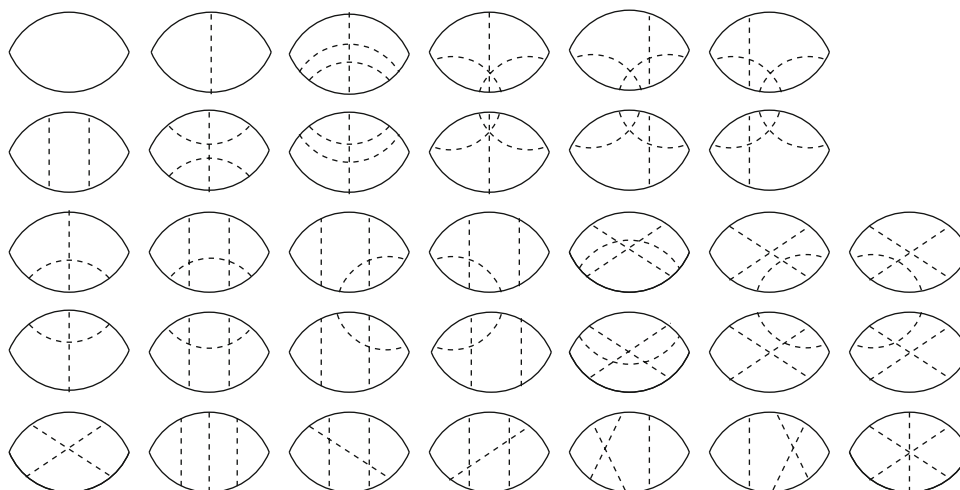


Fig. 6 Perturbative processes contributing to the dressing of the two-particle propagator up to the third-order in disorder strength. Solid lines denote the fully dressed Wegner’s propagators and the dashed lines the disorder correlators

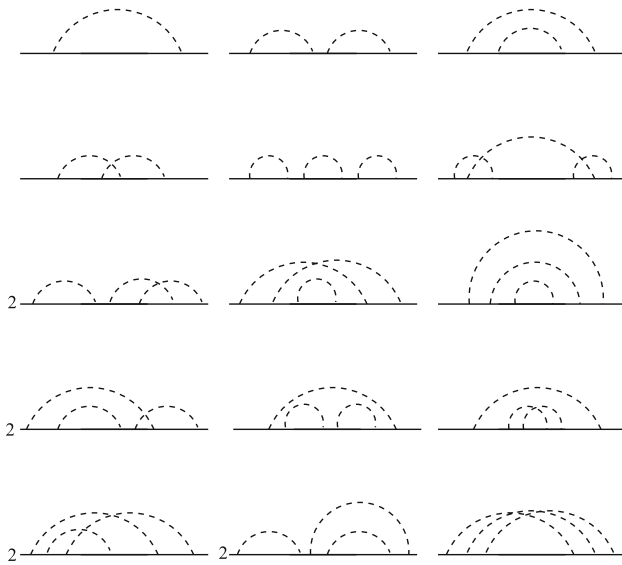


Fig. 7 Perturbative processes contributing to the dressing of the single-particle propagator due to the disorder to order g^1 (one diagram), g^2 (three diagrams), and g^3 (fifteen diagrams)

channel. The diagrams belonging to the so-called fan channel, e.g., no. 4, 17, etc., retain the same Gaussian exponent in every perturbative order. In Appendix 1, we argue that they contribute the least to the amplitudes in every order of expansion and therefore are clearly subdominant in comparison to the ladder channel.

Appendix C: Exact Wegner’s propagator of the disordered system

We start the discussion of the dressing effect for the single-particle propagator by evaluating all perturbative contributions to order g^2 and g^3 . The number of diagrams to order g^n , n being a positive integer number and zero is $\frac{(2n)!}{2^n n!}$; hence, there are in total three diagrams to the order g^2 and 15 diagrams to the order g^3 , Fig. 7. In Table 2, we summarize their amplitudes. Next order g^4 would require the evaluation of 105 diagrams with a larger computational effort for each individual diagram. To this end though, we have an asymptotically exact expression:

$$\bar{G}_{rr'}^\pm(E) = \frac{k^2}{\pi} e^{-\frac{k^2}{2}(|r|^2+|r'|^2-2\bar{r}r')} \sum_{s=\pm} \mathcal{P}_s \mathcal{F}_s^\pm(E), \tag{C1}$$

where the frequency-dependent part of the Green’s function reads

$$\mathcal{F}_s^\pm(E) = \frac{1}{2} \frac{1}{E - E_s} \left[1 + \frac{E_g^2}{[E - E_s]^2} + \frac{5}{2} \frac{E_g^4}{[E - E_s]^4} + \frac{37}{4} \frac{E_g^6}{[E - E_s]^6} \dots \right], \tag{C2}$$

where $E_g^2 = \frac{gk^2}{4\pi}$. Not surprisingly, the expansion coefficients 1, 1, 5/2, 37/4.. are precisely those of the exact solution by

Wegner Ref. [9], extended by Brézin et al. with a different technique in Ref. [10].

Following the line of Wegner’s reasoning, the series in the rectangular brackets in Eq. (C2) is related to the zero dimensional functional integral

$$\frac{1}{a} \sum_{n=0}^\infty f_n \left(-\frac{b}{a^2} \right)^n = \frac{\int d\phi^* d\phi \phi^* \phi e^{-a\phi^* \phi - \frac{b}{4}(\phi^* \phi)^2}}{\int d\phi^* d\phi e^{-a\phi^* \phi - \frac{b}{4}(\phi^* \phi)^2}}, \tag{C3}$$

with f_n representing the combinatorial factor. To ensure the convergence, the real part of a has to be positive. The integral can be carried out exactly by quadratic complement, giving

$$\frac{1}{a} \sum_{n=0}^\infty f_n \left(-\frac{b}{a^2} \right)^n = -\frac{\partial}{\partial a} \log \left[\frac{2\pi}{\sqrt{b}} e^{-\frac{a^2}{b}} \int_{\frac{a}{\sqrt{b}}}^\infty dt e^{-t^2} \right]. \tag{C4}$$

The integral under the logarithm is rewritten as

$$\int_{\frac{a}{\sqrt{b}}}^\infty dt e^{-t^2} = \frac{\sqrt{\pi}}{2} \left[1 - \frac{2}{\sqrt{\pi}} \int_0^{\frac{a}{\sqrt{b}}} dt e^{-t^2} \right], \tag{C5}$$

and therefore

$$\frac{1}{a} \sum_{n=0}^\infty f_n \left(-\frac{b}{a^2} \right)^n = -\frac{\partial}{\partial a} \log \left[e^{-\frac{a^2}{b}} \left(1 - \frac{2}{\sqrt{\pi}} \int_0^{\frac{a}{\sqrt{b}}} dt e^{-t^2} \right) \right] \tag{C6}$$

$$= \frac{2}{\sqrt{b}} \left[\frac{a}{\sqrt{b}} + \frac{1}{\sqrt{\pi}} \frac{e^{-\frac{a^2}{b}}}{1 - \frac{2}{\sqrt{\pi}} \int_0^{\frac{a}{\sqrt{b}}} dt e^{-t^2}} \right]. \tag{C7}$$

Plugging into this expression

$$a = \mp i [E - E_s \pm i0^+], \quad \text{and} \quad b = E_g^2, \tag{C8}$$

we get the frequency-dependent part of the propagator for each spectral mode of the lowest Landau level

$$\mathcal{F}_s^\pm(E) = -\frac{1}{2E_g} \left[2\nu_s \pm \frac{i}{\sqrt{\pi}} \frac{e^{\nu_s^2}}{1 \mp i \frac{2}{\sqrt{\pi}} \int_0^{\nu_s} dt e^{t^2}} \right], \tag{C9}$$

where $\nu_s = (E - E_s)/E_g$. From here, one obtains the real and imaginary parts of the Green’s function Eqs. (26) and (27) shown in Fig. 8. The imaginary part, which is essentially the contribution to the net density of states from each spectral mode in the lowest Landau level, is placed symmetrically around the Landau zero point with the maximum at the band center.

To Fourier transform the Wegner’s propagator with respect to the energy, we start with Eq. (C2) rewritten in

accord with Eq. (C3)

$$\mathcal{F}_s^\pm(E) = \mp \frac{i}{2} \frac{1}{\mp i(E - E_s)} \left[1 - \frac{E_g^2}{[\mp i(E - E_s)]^2} + \frac{5}{2} \frac{E_g^4}{[\mp i(E - E_s)]^4} - \frac{37}{4} \frac{E_g^6}{[\mp i(E - E_s)]^6} \dots \right]. \tag{C10}$$

Then, the leading order term is easily Fourier transformed with the help of the Cauchy theorem

$$\mp \int \frac{dE}{2\pi i} \frac{e^{\pm iEt}}{E - E_s \pm i0^+} = e^{\pm iE_s t}, \tag{C11}$$

with the contour integration stretching over the entire complex plane, and hence necessarily enveloping the pole. All higher terms follow essentially by taking derivatives of the oscillating function on the right hand side with respect to E_s , e.g.,

$$\int \frac{dE}{2\pi} \frac{e^{\pm iEt}}{[\mp i(E - E_s \pm i0^+)]^{2n+1}} = \mp \frac{(-1)^n}{2n!} \frac{\partial^{2n}}{\partial E_s^{2n}} \int \frac{dE}{2\pi i} \frac{e^{\pm iEt}}{E - E_s \pm i0^+} \tag{C12}$$

$$= \frac{(-1)^n}{2n!} \frac{\partial^{2n}}{\partial E_s^{2n}} e^{\pm iE_s t} = \frac{t^{2n}}{2n!} e^{\pm iE_s t}. \tag{C13}$$

This gives for the Fourier transformed Wegner’s function the following series:

$$\mathcal{F}_s^\pm(t) = \mp \frac{i}{2} e^{\pm iE_s t} \left[1 - \frac{(E_g t)^2}{2!} + \frac{5}{2} \frac{(E_g t)^4}{4!} - \frac{37}{4} \frac{(E_g t)^6}{6!} \dots \right]. \tag{C14}$$

The combinatorial factors of the series in the rectangular brackets can be determined to every order using the integral representation Eq. (C3). We therefore can write it as

$$\mathcal{F}_s^\pm(t) = \mp \frac{i}{2} e^{\pm iE_s t} \Omega(E_g t), \quad \Omega(E_g t) = \sum_{n=0}^\infty (-1)^n f_n \frac{(E_g t)^{2n}}{(2n)!}, \tag{C15}$$

where f_n denotes the combinatorial factors from Eq. (C3).

Appendix D: Evaluation of the mean-squared displacement: technical issues

After accounting for all processes which dress the single-particle Green’s propagators, the disorder effect for the two-particle propagator and correspondingly for the mean-squared displacement comes from the loop diagrams, which involve at least one scattering process between the advanced and retarded sides. All such diagrams to order g^3 are shown in Fig. 6. Every single diagram can be evaluated exactly in a very efficient way using the master formula Eq. (B1). The results for each diagram are summarized in Table 3. The appearance of the trigonometric cosine functions in some of the terms is due to the fact that the corresponding loop diagrams contain unequal numbers of advanced/retarded propagators. Each diagram in the respective class is then complex, but the sum of all complex conjugate diagrams is real and proportional to the cosine. Even numbers in the argument of the cosine are equal to the difference between the number of propagators in each side. Because our series contain only cosine functions, they might seem different in comparison to Refs. [11, 12, 27, 28]. There is no discrepancy though, since these authors use extensively the additional formulae of trigonometric functions, cf. especially Ref. [12].

Diagrams in every order organize in distinct subgroups by the topology of the diagrams. The sum of all terms in a subgroup is a real function. We summarize the results for every subgroup in expansion of the second moment of the position operator $\sum_r r_\mu^2 P_{r,0}$ in Table 3 and for the corresponding normalization $\sum_r P_{r,0}$ in Table 4. Each subgroup provides in the n th order of $\sum_r r_\mu^2 P_{r,0}$ for a contribution

$$\mathcal{R}_i^{(n)} = \frac{1}{4\pi} \frac{1}{E_g^2} \sum_s (2X_s)^{2n+2} \cos[(\mathcal{N}_i^+ - \mathcal{N}_i^-)\phi_s] \mathcal{C}_{2,i}^{(n)}, \tag{D1}$$

where $X_s^2 = E_g^2[\eta_s^2(E) + \rho_s^2(E)]$, $\phi_s = \arctan\left[\frac{\rho_s}{\eta_s}\right]$, and \mathcal{N}_i^\pm is the number of advanced (+) and retarder (−) propagators in the propagator, obeying $\mathcal{N}_i^+ + \mathcal{N}_i^- = 2n$, and i is the index of the subgroup as it appears in Tables 3 and 4. The corresponding expression for the normalization $\sum_r P_{r,0}$

Table 2 Amplitudes of each perturbative process contributing to the dressing of the single-particle propagator up to the order g^3 in multiples of $k^2/2\pi$

No.	Diagram	Amplitude	No.	Diagram	Amplitude	No.	Diagram	Amplitude
1		$\sum_s E_g F_s^3$	6		$\frac{1}{3} \sum_s E_g^3 F_s^7$	11		$\sum_s E_g^3 F_s^7$
2		$\sum_s E_g^2 F_s^5$	7		$\sum_s E_g^3 F_s^7$	12		$\frac{1}{2} \sum_s E_g^3 F_s^7$
3		$\sum_s E_g^2 F_s^5$	8		$\frac{1}{2} \sum_s E_g^3 F_s^7$	13		$\frac{2}{3} \sum_s E_g^3 F_s^7$
4		$\frac{1}{2} \sum_s E_g^2 F_s^5$	9		$\sum_s E_g^3 F_s^7$	14		$2 \sum_s E_g^3 F_s^7$
5		$\sum_s E_g^3 F_s^7$	10		$\sum_s E_g^3 F_s^7$	15		$\frac{1}{4} \sum_s E_g^3 F_s^7$

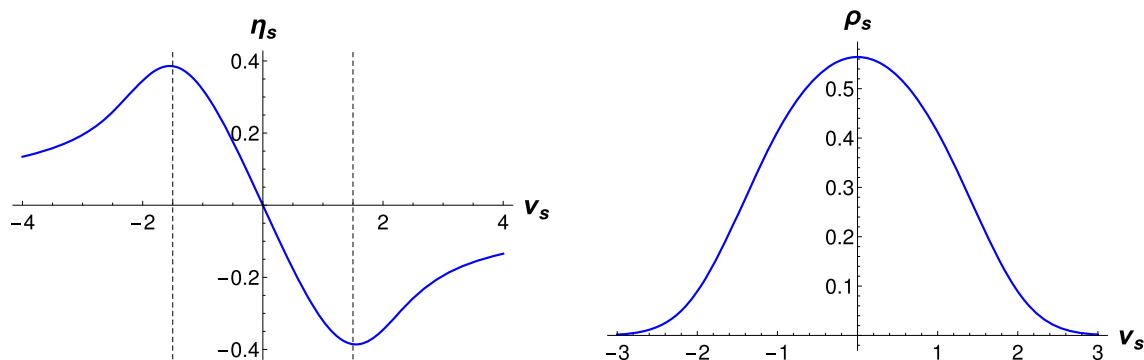


Fig. 8 The shape of the real (left) and imaginary (right) part of the Wegner’s propagator

Table 3 Amplitudes $C_{2,i}^{(n)}$ of every term of $\sum_r r_\mu^2 P_{r,0}$ up to the order g^3 , i is the number of the diagram. The net contribution from each diagram is acquired by inserting the elements of the Table into Eq. (D1). In every order, the ladder diagrams weight substantially heavier as all other non-oscillating terms (no. 4, 6, 15, 16, 17) combined

No.	Diagram	Amplitude	No.	Diagram	Amplitude	No.	Diagram	Amplitude
1		1/2	6		2/9	12		3/8
2		1	7		4/9	13		4/3
3		3/2	8		3/8	14		2
4		1/2	9		10/9	15		2/3
5		3/4	10		5/9	16		3/2
			11		5/2	17		1/4

Table 4 Amplitudes $C_{0,i}^{(n)}$ of every term of $\sum_r P_{r,0}$ up to the order g^3 , i is the number of the diagram. The net contribution for the respective expansion order from each diagrams is acquired by inserting the elements of the Table into Eq. (D2)

No.	Diagram	Amplitude	No.	Diagram	Amplitude	No.	Diagram	Amplitude
1		1	6		1/3	12		1/2
2		1	7		2/3	13		4/3
3		1	8		1/2	14		1
4		1/2	9		4/3	15		2/3
5		1	10		2/3	16		1
			11		2	17		1/4

reads

$$\mathcal{Z}_i^{(n)} = \frac{k^2}{4\pi E_g^2} \sum_s (2X_s)^{2n+2} \cos[(\mathcal{N}_i^+ - \mathcal{N}_i^-)\phi_s] C_{0,i}^{(n)}. \tag{D2}$$

The factors $\mathcal{N}_i^+ - \mathcal{N}_i^-$ can be read off directly from the Fig. 6 giving $\mathcal{N}_i^+ - \mathcal{N}_i^- = 0$ for $i = 1, 2, 3, 4, 6, 14, 15, 16, 17$, $\mathcal{N}_i^+ - \mathcal{N}_i^- = 2$ for $i = 5, 10, 11, 12, 13$, and finally $\mathcal{N}_i^+ - \mathcal{N}_i^- = 4$ for $i = 7, 8, 9$.

The combinatorial factors $C_{2,i}^{(n)}$ for each subgroup represent rational numbers which appear as the result of integration in the position space (all variables rescaled in units of k)

$$C_{2,i}^{(n)} = \int \frac{d^2r}{2\pi} r^2 e^{-r^2} \underbrace{\int \frac{d^2x}{\pi} \dots \int \frac{d^2y}{\pi} \dots}_{n \text{ integrals}}, \tag{D3}$$

where the additional factor $1/2$ in the very first integral is due to the angular average $\langle r_\mu^2 \rangle_\varphi = 1/2 \langle r^2 \rangle_\varphi$. These integral

chains are unique for each diagram. Correspondingly, the combinatorial factors $C_{0,i}^{(n)}$ for the normalization are defined as

$$C_{0,i}^{(n)} = \int \frac{d^2r}{\pi} e^{-r^2} \underbrace{\int \frac{d^2x}{\pi} \dots \int \frac{d^2y}{\pi} \dots}_{n \text{ integrals}} \quad (D4)$$

There is a simple relation between $C_{2,i}^{(n)}$ and $C_{0,i}^{(n)}$

$$C_{0,i}^{(n)} = 2\chi_i C_{2,i}^{(n)}, \quad (D5)$$

where χ_i are taken from the Table 1. The combinatorial factors $C_{2,i}^{(n)}$ and $C_{0,i}^{(n)}$ for every term are summarized in Tables 3 and Table 4, respectively.

The inspection of the Gaussian exponents in Table 1 suggests that the dominant contribution on large scales in every order of expansion arises from the so-called ladder diagrams, i.e., diagrams no. 1, 2, 3, 14, etc. According to Table 3, they provide more weight in every order of expansion of $\sum_r r_\mu^2 P_{r0}$ than all other non-oscillating diagrams (without cosine) combined. In particular, the so-called fan diagrams, e.g., no. 4, 17, etc. contribute the least in every order of expansion. This is the ultimate reason for neglecting the contributions from the latter. Four lowest order ladder diagrams are

$$\begin{aligned} \bigcirc &= \frac{1}{4E_g^2} \left(\frac{k^2}{\pi}\right)^2 \sum_{s=\pm} (2X_s)^2 \exp[-k^2 r^2], \\ \bigcirc \text{ with dot} &= \frac{1}{4E_g^2} \left(\frac{k^2}{\pi}\right)^2 \sum_{s=\pm} \frac{(2X_s)^4}{2} \exp\left[-\frac{k^2 r^2}{2}\right], \end{aligned} \quad (D6)$$

$$\begin{aligned} \bigcirc \text{ with two dots} &= \frac{1}{4E_g^2} \left(\frac{k^2}{\pi}\right)^2 \sum_{s=\pm} \frac{(2X_s)^6}{3} \exp\left[-\frac{k^2 r^2}{3}\right], \\ \bigcirc \text{ with three dots} &= \frac{1}{4E_g^2} \left(\frac{k^2}{\pi}\right)^2 \sum_{s=\pm} \frac{(2X_s)^8}{4} \exp\left[-\frac{k^2 r^2}{4}\right], \end{aligned} \quad (D7)$$

which suggests the following approximate expression for the two-particle propagator:

$$P_{r0}^{\text{lad}}(E) \approx \frac{1}{4E_g^2} \left(\frac{k^2}{\pi}\right)^2 \sum_{s=\pm} \sum_{n=0}^{\infty} \frac{(2X_s)^{2n+2}}{n+1} \exp\left[-\frac{k^2 r^2}{n+1}\right]. \quad (D8)$$

The dominant oscillating correction comprises the menora diagrams no. 5, 7, etc., Table 1. The contribution from the diagrams 5 to the two-particles propagator reads

$$\bigcirc \text{ with four dots} = \frac{1}{4E_g^2} \left(\frac{k^2}{\pi}\right)^2 \sum_{s=\pm} \frac{2}{3} \exp\left[-\frac{2}{3}k^2 r^2\right] (2X_s)^6 \cos 2\phi_s, \quad (D9)$$

from the diagrams 7

$$\bigcirc \text{ with five dots} = \frac{1}{4E_g^2} \left(\frac{k^2}{\pi}\right)^2 \sum_{s=\pm} \frac{2}{4} \exp\left[-\frac{3}{4}k^2 r^2\right] (2X_s)^8 \cos 4\phi_s, \quad (D10)$$

and so on. The full series accounting for the contribution from the menora channel then becomes

$$P_{r0}^{\text{men}}(E) = \frac{2}{4E_g^2} \left(\frac{k^2}{\pi}\right)^2 \sum_{s=\pm} \sum_{n=2}^{\infty} \frac{(2X_s)^{2n+2}}{n+1} \cos[(2n-2)\phi_s] \exp\left[-\frac{n}{n+1}k^2 r^2\right]. \quad (D11)$$

Both ladder and menora channels combined represent a reasonable exact large-scale asymptotics for the dressed two-particle propagator.

Appendix E: Details of the derivation of Eq. (50)

We begin with Eq. (49) and use the fluctuations $\langle \delta f^{(i)} \rangle$ as the generators of the time evolution of the mean-squared displacement at small positive/negative times Δt :

$$\begin{aligned} k^2 \langle r_\mu^2(\pm \Delta t) \rangle &= \langle f^{(2)} \rangle + \sum_{s=\pm} \int_{-\infty}^{\infty} d\nu_s \left[e^{\pm i\nu_s E_g \Delta t} - 1 \right] \frac{N}{2} (2X_s)^{2N} \\ &\approx \frac{\langle f^{(0)} \rangle + \sum_{s=\pm} \int_{-\infty}^{\infty} d\nu_s \left[e^{\pm i\nu_s E_g \Delta t} - 1 \right] (2X_s)^{2N}}{\langle f^{(0)} \rangle + \sum_{s=\pm} \int_{-\infty}^{\infty} d\nu_s \left[e^{\pm i\nu_s E_g \Delta t} - 1 \right] (2X_s)^{2N}}, \end{aligned} \quad (E1)$$

where we carry out the Fourier transform in the energy units specific for the time representation of the Wegner's propagator Eq. (30). Obviously, the case $\Delta t = 0$ restores Eq. (E1). For small $(e^{\pm i\nu_s E_g \Delta t} - 1)$ we have

$$\begin{aligned} k^2 [\langle r_\mu^2(\pm \Delta t) \rangle - \langle r_\mu^2(0) \rangle] &\approx \frac{1}{\langle f^{(0)} \rangle} \sum_{s=\pm} \int_{-\infty}^{\infty} d\nu_s \\ &\left[e^{\pm i\nu_s E_g \Delta t} - 1 \right] (2X_s)^{2N} \left[\frac{N}{2} - k^2 \langle r_\mu^2(0) \rangle \right]. \end{aligned} \quad (E2)$$

Summing both sides yields

$$\begin{aligned} k^2 [\langle r_\mu^2(\Delta t) \rangle - 2\langle r_\mu^2(0) \rangle + \langle r_\mu^2(-\Delta t) \rangle] &= \frac{2}{\langle f^{(0)} \rangle} \sum_{s=\pm} \int_{-\infty}^{\infty} d\nu_s [\cos(\nu_s E_g \Delta t) - 1] \\ &\times (2X_s)^{2N} \left[\frac{N}{2} - k^2 \langle r_\mu^2(0) \rangle \right]. \end{aligned} \quad (E3)$$

$$\quad \times (2X_s)^{2N} \left[\frac{N}{2} - k^2 \langle r_\mu^2(0) \rangle \right]. \quad (E4)$$

Taking the limit $\Delta t \rightarrow 0$ and using the self-consistent approximation yield Eq. (50).

References

1. A.H. Castro Neto, F. Guinea, N.M.R. Peres, K.S. Novoselov, A.K. Geim, The electronic properties of graphene. Rev. Mod. Phys. **81**, 109 (2009)
2. M.Z. Hasan, C.L. Kane, Colloquium: topological insulators. Rev. Mod. Phys. **82**, 3045 (2010)
3. V.N. Kotov, B. Uchoa, V.M. Pereira, F. Guinea, A.H. Castro Neto, Electron-electron interactions in graphene: current status and perspectives. Rev. Mod. Phys. **84**, 1067 (2012)

4. X.-L. Qi, S.-C. Zhang, Topological insulators and superconductors. *Rev. Mod. Phys.* **83**, 1057 (2011)
5. D. Culcer, A.C. Keser, Y. Li, G. Tkachov, Transport in two-dimensional topological materials: recent developments in experiment and theory. *2D Materials* **7**, 022007 (2020)
6. A. Avsar, H. Ochoa, F. Guinea, B. Özyilmaz, B.J. van Wees, I.J. Vera-Marun, Colloquium: spintronics in graphene and other two-dimensional materials. *Rev. Mod. Phys.* **92**, 021003 (2020)
7. M. König, H. Buhmann, L.W. Molenkamp, T. Hughes, C.-X. Liu, X.-L. Qi, S.-C. Zhang, The quantum spin hall effect: theory and experiment. *J. Phys. Soc. Jpn.* **77**, 031007 (2008)
8. T. Ando, Theory of quantum transport in a two-dimensional electron system under magnetic field. III. Many-site approximation, *J. Phys. Soc. Jpn.* **37**, 622 (1974)
9. F.J. Wegner, Exact density of states for lowest Landau level in white noise potential. Superfield representation for interacting systems, *Z. Phys. B Cond. Mat.* **51**, 279 (1983)
10. E. Brézin, D.J. Gross, C. Itzykson, Density of states in the presence of a strong magnetic field and random impurities. *Nucl. Phys. B* **235**, 24 (1984)
11. S. Hikami, Borel-Padé analysis for the two-dimensional electron in a random potential under a strong magnetic field. *Phys. Rev. B* **29**, 3726(R) (1984)
12. S. Hikami, Anderson Localization of the two-dimensional electron in a random potential under a strong magnetic field. *Prog. Theor. Phys* **72**, 722 (1984)
13. H. Aoki, Quantised Hall effect. *Rep. Prog. Phys.* **50**, 655 (1987)
14. E. Abrahams, P.W. Anderson, D.C. Licciardello, T.V. Ramakrishnan, Scaling theory of localization: absence of quantum diffusion in two dimensions. *Phys. Rev. Lett.* **42**, 673 (1979)
15. L.G. Gor'kov, A.I. Larkin, D.E. Khmel'nitskii, Particle conductivity in a two-dimensional random potential, *Pis'ma Zh. Eksp. Teor. Fiz.* **30**, 248 (1979) [*JETP Lett.* **30**, 228 (1979)]
16. S. Hikami, A. Larkin, Y. Nagaoka, Spin-orbit interaction and magnetoresistance in the two dimensional random system. *Prog. Theor. Phys.* **63**, 707 (1980)
17. F. Wegner, The mobility edge problem: continuous symmetry and a conjecture. *Z. Physik B* **35**, 207 (1979)
18. L. Schäfer, F. Wegner, Disordered system with n orbitals per site: lagrange formulation, hyperbolic symmetry, and Goldstone modes. *Z. Physik B* **38**, 113 (1980)
19. S. Hikami, Anderson localization in a nonlinear- σ -model representation. *Phys. Rev. B* **24**, 2671 (1981)
20. G. Tkachov, Topological insulators: the physics of spin helicity in quantum transport. Pan Stanford (2015)
21. A. Sinner, K. Ziegler, Two-parameter scaling theory of transport near a spectral node. *Phys. Rev. B* **90**, 174207 (2014)
22. A. Sinner, K. Ziegler, Finite-size scaling in a 2D disordered electron gas with spectral nodes. *J. Phys. Cond. Mat.* **28**, 305701 (2016)
23. N. Goldenfeld, *Lectures on phase transitions and the renormalization group* (Perseus Books, Reading, Massachusetts, 1992)
24. K. Huang, *Statistical mechanics*, 2nd edn. (John Wiley, New York, 1987)
25. P.M. Chaikin, T.C. Lubenski, *Principles of condensed matter physics* (Cambridge University Press, Cambridge, 1995)
26. K. Ziegler, Quantum diffusion in two-dimensional random systems with particle-hole symmetry. *J. Phys. A Math. Theor.* **45**, 335001 (2012)
27. R.R.P. Singh, S. Chakravarty, A disordered two-dimensional system in a magnetic field: Borel-Padé analysis. *Nucl. Phys. B* **265**, 265 (1986)
28. S. Hikami, M. Shirai, F.J. Wegner, Anderson localization in the lowest Landau level for a two-subband model. *Nucl. Phys. B* **408**, 415 (1993)
29. B.A. Bernevig, T.L. Hughes, S.-C. Zhang, Quantum spin Hall effect and topological phase transition in HgTe quantum wells. *Science* **314**, 1757 (2006)
30. G. Li, E.Y. Andrei, Observation of Landau levels of Dirac fermions in graphite. *Nat. Phys.* **3**, 623 (2007)
31. K.S. Novoselov, A.K. Geim, S.V. Morozov, D. Jiang, M.I. Katsnelson, I.V. Grigorieva, S.V. Dubonos, A.A. Firsov, Two-dimensional gas of massless Dirac fermions in graphene. *Nature* **438**, 197 (2005)
32. Z. Jianga, Y. Zhanga, Y.-W. Tana, H.L. Stormer, P. Kim, Quantum Hall effect in graphene. *Sol. State Com.* **143**, 14 (2007)
33. P. Goswami, X. Jia, S. Chakravarty, Quantum Hall plateau transition in the lowest Landau level of disordered graphene. *Phys. Rev. B* **76**, 205408 (2007)
34. F.J. Wegner, Disordered system with n orbitals per site: $n = \infty$ limit. *Phys. Rev. B* **19**, 783 (1979)
35. Y. Huo, R.E. Hetzel, R.N. Bhatt, Universal conductance in the lowest Landau level. *Phys. Rev. Lett.* **70**, 481, 031007 (1993)
36. A.J. McKane, M. Stone, Localization as an alternative to Goldstone's theorem. *Ann. Phys.* **131**, 36 (1981)
37. A.W.W. Ludwig, M.P.A. Fisher, R. Shankar, G. Grinstein, Integer quantum Hall transition: an alternative approach and exact results. *Phys. Rev. B* **50**, 7526, 031007 (1994)
38. B.L. Altshuler, B.D. Simons, Universalities: From Anderson localization to quantum chaos. In *Mesoscopic quantum physics, Les Houches 1994*, Akkermans, E.; Montambaux, G.; Pichard, J.-L.; Zinn-Justin, J. North Holland, Amsterdam, Netherlands, pp. 1-98 (1995)
39. K. Efetov, *Supersymmetry in disorder and chaos* (Cambridge University Press, Cambridge, 1997)
40. E. Fradkin, Critical behavior of disordered degenerate semiconductors. II. Spectrum and transport properties in mean-field theory. *Phys. Rev. B* **33**, 3263 (1986)
41. V.P. Sharapov, S.G. Gusynin, Transport of Dirac quasiparticles in graphene: hall and optical conductivities. *Phys. Rev. B* **73**, 245411 (2006)
42. K. Ziegler, Robust transport properties in graphene. *Phys. Rev. Lett.* **97**, 266802 (2006)
43. K. Ziegler, Minimal conductivity of graphene: nonuniversal values from the Kubo formula. *Phys. Rev. B* **75**, 233407 (2007)
44. A. Sinner, K. Ziegler, Conductivity of disordered 2d binodal Dirac electron gas: effect of internode scattering. *Phil. Mag.* **98**, 1799 (2018)